

Deep learning based surrogate models for first-principles global simulations of fusion plasmas

G. Dong^{1,a,*}, X. Wei^{2,a}, J. Bao³, G. Brochard², Z. Lin² and W. Tang¹

¹ Princeton Plasma Physics Laboratory, Princeton, NJ, United States of America

² University of California, Irvine, Irvine, CA, United States of America

³ Institute of Physics, Chinese Academy of Sciences, Beijing 100190, China

E-mail: gdong@princeton.edu

Received 15 July 2021, revised 4 October 2021

Accepted for publication 25 October 2021

Published 18 November 2021



Abstract

The accurate identification and control of plasma instabilities is important for successful fusion experiments. First-principle simulations that can provide physics-based instability information such as the mode structure are generally not fast enough for real-time applications. In this work, a workflow has been presented to develop deep-learning based surrogate models for the first-principle simulations using the gyrokinetic toroidal code (GTC). The trained surrogate models of GTC (SGTC) can be used as physics-based fast instability simulators that run on the order of milliseconds, which fits the requirement of the real-time plasma control system. We demonstrate the feasibility of this workflow by first creating a big database from GTC systematic linear global electromagnetic simulations of the current-driven kink instabilities in DIII-D plasmas, and then developing SGTC linear internal kink instability simulators through supervised training. SGTC linear internal kink simulators demonstrate predictive capabilities for the mode instability properties including the growth rate and mode structure.

Keywords: plasma physics, kink mode, neural network, artificial intelligence

(Some figures may appear in colour only in the online journal)

1. Introduction

In real-time toroidal plasma experiments, accurate physics-based information of plasma instabilities can provide important guidance for successful plasma control [1]. For example, the neoclassical tearing mode (NTM) [2] is one of the most commonly observed causes for plasma major disruption [3], which is the abrupt loss of plasma confinement accompanied by large instantaneous energy transport that can damage the experimental device, especially for larger future tokamaks. The identification, predictions and control of the plasma perturbations that can excite NTM, such as the sawtooth oscillations [4, 5], form the basis for effective NTM control

and early disruption alarms. ITER is the next-step international toroidal fusion reactor towards unlimited carbon-free energy [6]. Currently, the construction and design of ITER operations and the plasma control system (PCS) are partially dependent on the empirical extrapolation of instabilities, transport and other confinement properties from smaller experimental devices around the world [1, 7]. First-principles based study of plasma instabilities can improve the understanding and prediction of the dynamics and transport at the plasma core [8, 9] and plasma edge [10, 11] in future fusion devices such as ITER. Plasma instabilities such as magnetohydrodynamic (MHD) modes, micro-turbulence and alfvén eigenmodes are widely studied with the utilization of various types of physics models and computational algorithms, including fluid MHD codes [12, 13], gyrokinetic Eulerian codes [14, 15], gyrokinetic particle-in-cell codes [16, 17] and etc. While these physics-based simulations can provide accurate growth rate,

* Author to whom any correspondence should be addressed.

^a These authors contributed equally to this work.

mode structure, and driving mechanisms for various plasma instabilities in their linear [18] and nonlinear stage [19] for realistic experimental equilibrium, the first-principles simulations can be expensive computationally. Simulation time for physical instabilities using gyrokinetic particle-in-cell codes is often on the order of hours on modern GPUs [20], making the direct application of these codes in real-time experiments infeasible.

On the other hand, statistical methods including machine learning models have been applied in the PCS to predict plasma behaviors [21–23]. Recently deep-learning based models have achieved promising results in disruption predictions [23], the prediction of perturbed magnetic signals [22–24], and building emulators to aid first-principles simulations [25]. Compared with classical machine learning models, deep-learning based models are built in layered fashion and the number of layers can become large as the model becomes ‘deeper’. In this paper we present a workflow to build a deep-learning based surrogate model as a fast physics-based instability simulator. Here, surrogate models of the first-principles simulations are deep-learning models that runs (or inferences) on a sub-millisecond time scale, and can output results representing those from the first-principles simulations. We show the first results from deep-learning models trained based on data from linear global gyrokinetic toroidal code (GTC), which has performed thousands of electromagnetic simulations in the fluid limit by suppressing all kinetic effects and using the DIII-D experimental equilibria. As an initial investigation in this area, we have trained the surrogate models on GTC simulation results of the linear internal kink modes, which are commonly observed [26–28] current driven MHD instabilities that are closely related to the sawtooth activities [29], fishbone modes [30, 31], and NTMs [32]. Compared with the hours-scale gyrokinetic simulation time of GTC with kinetic effects for the internal kink mode, the inference time of the surrogate model of GTC (SGTC) is on the order of milliseconds, which fits the requirement of the DIII-D real-time PCS. SGTC demonstrates predictive capabilities of the linear kink mode instability properties including the mode growth rate and mode structure. The output of SGTC contains physics-based linear instability properties that can complement experimental measurements and provide more targeted guidance to the PCS. SGTC can also serve as a physical simulator in other plasma predictive algorithms, enabling the development of future AI-based plasma control algorithms. At this stage, the SGTC kink simulators are based on the linear global GTC simulations and therefore the results shown in section 4 are not applicable in making predictions for the nonlinear dynamics of the kink modes, and some of the predicted linear mode properties cannot be compared with experimental measurements directly. The development of nonlinear capabilities is undergoing and future work.

In the rest of this paper, we introduce the design and workflow of SGTC in section 2, followed by the data properties and GTC simulations of the linear onsets of the internal kink instabilities in section 3, and finally we present the training details and predictive performance of SGTC models, comparing SGTC and GTC outputs in section 4.

2. Deep learning based surrogate model of GTC (SGTC)

The design workflow of SGTC is shown in figure 1. As shown by the deep blue solid arrows in the left panel, experimentally measured signals including the zero-dimensional scalar signals such as plasma core density, one-dimensional profile signals such as the plasma density profile, and two-dimensional signals such as the magnetic field, are used as inputs to SGTC. The inputs can easily be extended to higher dimensional measurements in future work. SGTC then outputs the plasma instability information, such as the mode growth rate, frequency, and global mode structure as illustrated by the perturbation snapshot in DIII-D plasma poloidal plane shown in the lower left panel. The instability properties can in turn be used in the PCS as inputs to control algorithms, as shown by the red arrow. SGTC output can also be fed to plasma predictive models, which then output plasma state predictions to the PCS. SGTC architecture is shown in the green box in the right panel. The zero-dimensional features are input to Nf1 fully connected layers, which outputs the zero-dimensional features. The high dimensional inputs are fed into a set of Nc convolutional layers with dropout layers, and then Nf2 fully connected layers. The fully connected layers are standard linear operations for feature transformation and information extraction. The convolutional layers are used for more efficient feature extraction from the high-dimensional inputs. The combined use of the convolutional and fully connected layers can provide improved modeling capabilities [33]. The outputs from the fully connected layers are the high dimensional features that will be concatenated with the zero-dimensional features, and then goes through the fully connected output layers. For mode stability and growth rate prediction models, the output dimension is 1, and for poloidal mode structure prediction models, the output dimension is $M_\psi * M_\theta$, where M_ψ is the radial grid number, and M_θ is the poloidal grid number. The hyperparameter tuning processes of this network will be introduced in section 4.

As shown on the right-hand side in figure 1, utilizing an ‘input tuner’ and an ‘output analyzer’ that will be introduced in detail in the next section, GTC first-principles simulation data are generated and used for training, validation and testing of SGTC. GTC is a global gyrokinetic simulation tool that has been developing since 1995 [34], and has been validated for simulations of different types of plasma instabilities in DIII-D, JET, EAST, KSTAR, HL-2A tokamaks, W7-X and LHD stellarators, and C2 field-reversed configuration. The first-principles GTC simulations with associated theory and experimental observations have led to scientific discovery in turbulence self-regulation by zonal flows [16], zonal flow damping [35], neoclassical transport [36], transport scaling [8], wave-particle decorrelation [37], energetic particle transport [38], electron transport [39], nonlinear dynamics of Alfvén eigenmodes [40], localization of Alfvén eigenmodes [41], drift-wave stability [42], transport bifurcation [43] in fusion plasmas. Its simulation of current driven kink instability [44] has recently been benchmarked against different codes [45]. In this study, we utilize GTC to create a database of the internal kink instabilities in DIII-D plasmas.

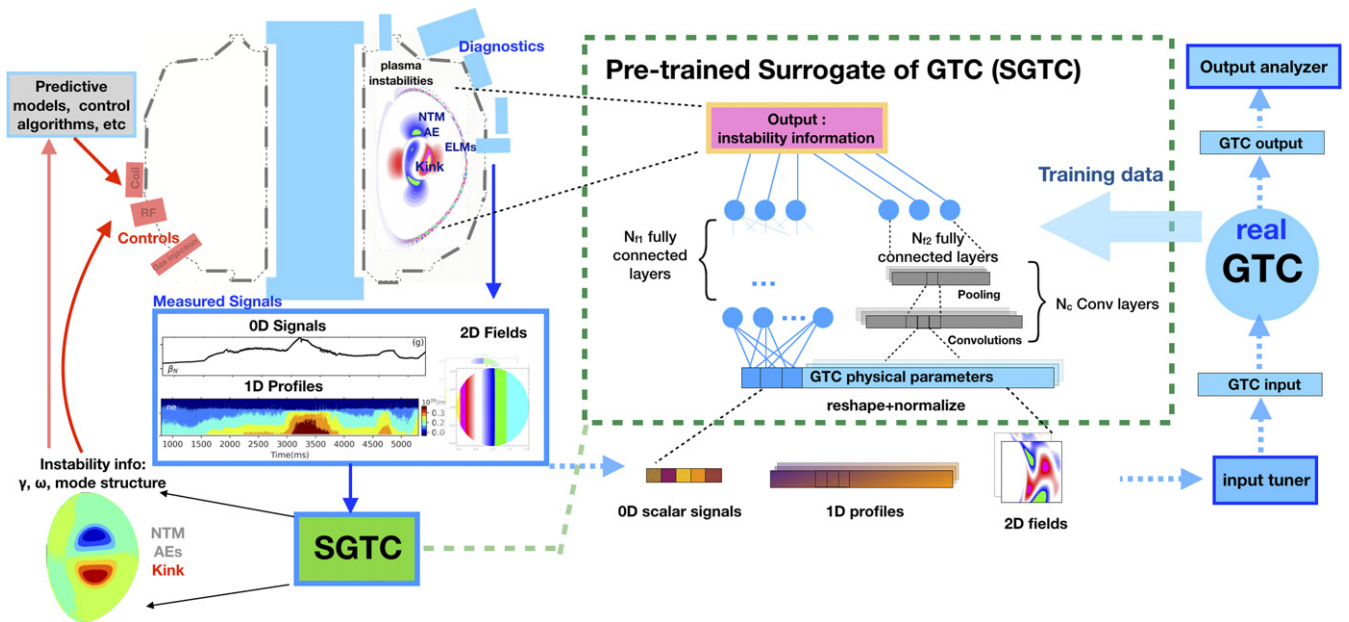


Figure 1. The workflow of SGTC. Measured signals are used as inputs to SGTC as shown by the deep blue solid arrows. SGTC then outputs the plasma instability information, such as the mode growth rate, frequency, and global mode structure as illustrated by the perturbation snapshot in DIII-D plasma poloidal plane. The instability properties can in turn be used in the PCS as inputs to control algorithms, as shown by the red arrow. SGTC output can also be fed to plasma predictive models, which then output plasma state predictions to the PCS. SGTC architecture is shown in the green box in the right panel. GTC data are generated and used for training, validation and testing of SGTC.

As the first-step towards synthetic instability simulations, we run GTC electromagnetic linear simulations of the non-tearing $n = 1$ instabilities in the ideal MHD limit with equilibrium current and compressible magnetic perturbations [46, 47], where n is the toroidal mode number, for 5758 equilibria selected from DIII-D experiments from magnetic EFIT01 [48] and motional stark effect (MSE) EFIT02 [49]. The complete GTC electromagnetic formulation is described in detail separately in [50]. GTC gyrokinetic simulation model reduces to the ideal MHD model by assuming zero resistivity, long wavelength, low beta and adiabatic electron response. The formulation of the MHD simulations in this study is derived and presented in section 2.4 in [50]. The GTC ideal MHD simulation is verified and validated using DIII-D shot #141216 [45], where a long-lived internal kink mode is identified experimentally. In [45] it is shown that the mode structures from the linear ideal MHD simulation quantitatively agree with electron cyclotron emission measurements with a corrected q profile. After completing GTC runs, we then performed supervised training of SGTC models with these DIII-D equilibria and GTC output data. In most of the GTC simulations finding unstable modes, the mode structures resemble those of the internal kink modes with dominant $m = 1$ component in electrostatic potential near the $q = 1$ rational surface [51], where m is the poloidal mode number, and q is the plasma safety factor. In the following text, we refer to the $n = 1$ MHD instabilities in GTC and SGTC outputs as the kink instabilities or the kink modes. SGTC models trained for these data can be considered as internal kink mode simulators for DIII-D plasmas.

3. Data and GTC simulations

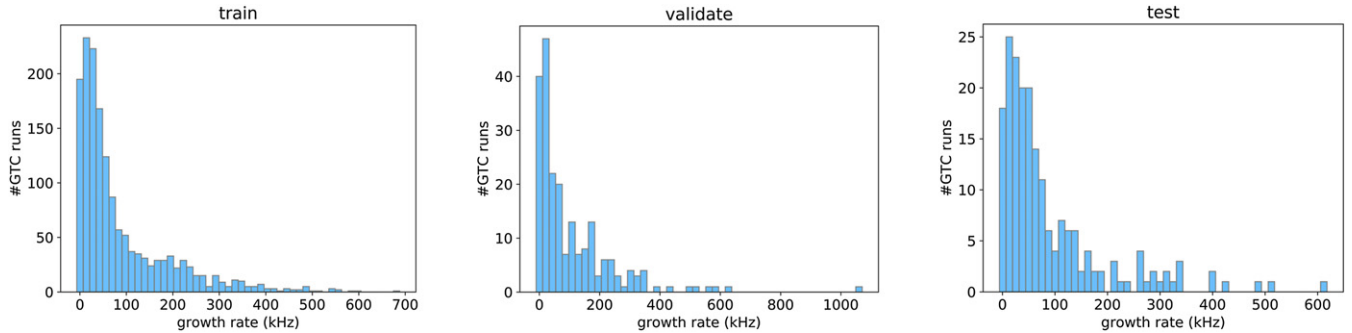
A list of DIII-D archived data that are used as GTC inputs are shown in table 1. Time sliced data are selected randomly from shot # 139520 to shot # 180844, with the condition that the listed data are available, and internal kink mode is possibly present at the time slice of interest. The presence of possible internal kink mode is determined from the combination of measured magnetic perturbations from the Mirnov coils and the minimum safety factor q_{\min} from EFIT [48]. EFIT02 data usually provide finer magnetic pitch angle (i.e. safety factor q) information, as it includes input information from the MSE diagnostics [52]. Among the 5758 DIII-D equilibria we simulated for this work, 2872 are based on magnetic EFIT01 output, and 2886 are based on MSE EFIT02 output. These simulations have been carried out in 12 GTC runs, each simulating 500 DIII-D experiments in parallel using 2000 nodes of the Summit supercomputer at ORNL for about 30 min (Summit has about 4700 nodes).

As shown by the GTC data generation workflow on the right of the dashed green box in figure 1, we first use an ‘input tuner’ to generate GTC inputs from experimental data. In this step we utilized the ORBIT code [53] to convert equilibrium data to Boozer coordinates.

With the inputs, global GTC electromagnetic simulations in the MHD limit are run for each input (i.e. each equilibrium of the DIII-D experiments) for 3000 time steps, with time step size $0.01 \frac{R_0}{C_s}$, where R_0 is the major radius and $C_s = \sqrt{T_e/m_i}$ is the ion sound speed with T_e as the on-axis electron temperature and m_i as the ion mass. Typical total simulation time

Table 1. List of DIII-D experimental data used as inputs for GTC simulations. Magnetic perturbation signals are only used for the selection of equilibriums.

Shot number	Data
5758 equilibriums from shot # 139520–180844	EFIT01 gfile EFIT02 gfile ZIPFIT01 electron temperature profile ZIPFIT01 electron density profile ZIPFIT01 ion temperature profile Magnetic perturbation (mpi66M307D) Magnetic perturbation (mpi66M322D)

**Figure 2.** Histogram of the kink growth rate from GTC simulations in training (left), validation (middle) and test (right) dataset. Simulation results with stable internal kink mode are not plotted.

for each equilibrium is on the order of 0.1 ms for the physical duration of the experiments.

After completing GTC simulations, we used an ‘output analyzer’ to examine the output data, exclude numerical instabilities, and prepare proper target data such as the mode growth rate, and poloidal eigenmode structure for SGTC. For results from each GTC simulation corresponding to a DIII-D equilibrium, the $n = 1$ mode growth rate is calculated with a linear fit of the perturbed parallel vector potential from the last 1000 time steps of the simulation. If there is no significant mode growth during the given time window, the equilibrium is linearly kink stable. On the other hand, if the growth rate is positive, the equilibrium is linearly unstable or the simulation is considered numerically unstable. To check numerical instabilities, the perturbed potential variation near $q = 1$ surface is analyzed. There are two criteria for a ‘physically’ unstable signal. Firstly, the mode should have nearly zero frequency. Secondly there should not be significant phase change, i.e. the mode does not rotate in poloidal and toroidal direction. If the simulation result does not meet both of the two criteria, the simulation is considered numerically unstable and this data point is dropped. After dropping the numerically unstable cases, we have comparable numbers of stable and unstable cases. Note that the ‘output analyzer’ is an important part of the workflow, since it performs preconditioning of the raw simulation results, contains the important physical standards for the phenomena of interest, and establishes the training database for the SGTC neural network.

In statistical learning, it is standard practice to divide the data into training, validation and testing sets, where the training data is used to fit the model. The validation set is

also given to the model in the training and hyperparameter selection phase, to provide a standard of the model performance, and prevent over fitting on the training set. The test set is unseen to the model, until the training and hyperparameter selection processes are done, to evaluate the final model predictive capability on new data. Among the 5758 DIII-D equilibria that GTC simulated in this study, 1972 equilibria have unstable $n = 1$ kink modes, 2531 equilibria are linearly stable for kink modes, and the remaining equilibria exhibit numerical instability. GTC simulation results of all the 1972 unstable cases and 2531 stable cases are used for training (80% of the data), validation (10% of the data), and testing (10% of the data) of SGTC. The histogram of the unstable mode growth rate in training, validation and testing dataset for the neural networks are shown in figure 2. Since the simulations are in the ideal MHD limit without kinetic effects, the linear growth rate can be large, for example above 400 kHz. The distribution of the mode instability in physical parameter space is shown in figure 3. The x axis $r(q = 1)$ denotes the minor radius of the $q = 1$ surface. The y axis in figure 3 is defined as $\delta\beta_p = -\frac{R_0^2 \int_{r_1}^{r_1} p' r^2 dr}{B_0^2 r_1^4}$, where r_1 denotes the minor radius of the $q = 1$ surface, p' denotes the radial derivative of the plasma pressure profile, and B_0 denotes the toroidal magnetic field. $\delta\beta_p$ is a relevant parameter for the kink instability in linear ideal MHD theory [54]. We investigated the data distribution on other parameters, e.g. magnetic shear, plasma beta, pressure gradient, and minimum value of q profile, and found that the $q = 1$ surface location and $\delta\beta_p$ are the two parameters most relevant to the stability of internal kink mode [50]. It is possible to use machine learning algorithm to find two parameters which better separate the stable and unstable cases than

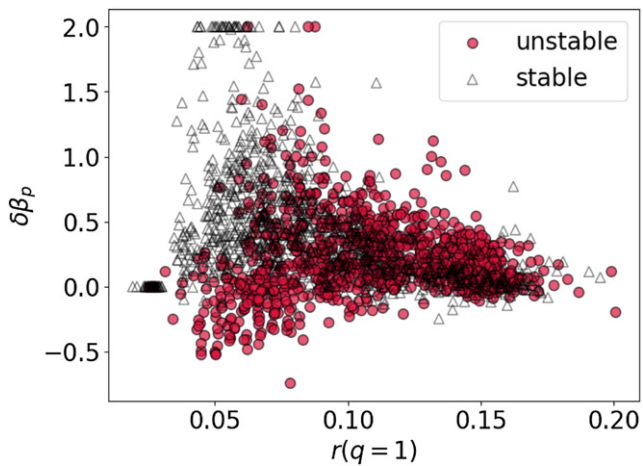


Figure 3. Kink instability distribution in parameter space from GTC simulations.

in figure 3, but normally it is very difficult to find the physical meanings of such automatically generated parameters. Therefore, we use $r(q=1)$ and $\delta\beta_p$ with clear physical meanings in figures 3 and 5.

4. Training and performance of SGTC

In SGTC internal kink simulators, we trained neural networks to predict the mode instability (which is a binary value to indicate whether the equilibrium of interest is kink unstable), mode growth rate, and two dimensional poloidal mode structure. The first predictive task of SGTC is the prediction of mode instability. In addition to deep learning (DL) based models, we also tested the performance of classical algorithms in which models cannot be easily extended in a stacked layers fashion. In figure 4, we show comparison of the predictive capabilities of the neural networks and of the classical algorithms. Inputs of the models are described in section 2, and the output of the model is an instability score. When the instability score is above a certain threshold, the mode is considered unstable, and otherwise considered stable. The instability threshold can be varied to achieve a receiver operating characteristic (ROC) curve for each model as shown in figure 4, where the y-axis is the true positive rate (TPR) defined as the number of correctly predicted unstable cases divided by the number of all unstable cases, and the x-axis is the false positive rate (FPR) defined as the number of stable cases which are incorrectly predicted as unstable, divided by the number of all stable cases. We used the area under the ROC curve (AUC) as the metric to evaluate model performance.

We trained multiple classical models in the sklearn package, and the best performing one is the random forest (RF) model [55]. We hand-tuned both the RF model and the neural network for the instability prediction on the validation dataset, and reported the ROC curve on the test dataset. The AUC for the DL based model and the RF model on the test dataset are 0.945 and 0.927 respectively. Figure 4 shows that the neural network outperforms the RF model near the optimal threshold regime, where on the ROC curve the distance to the upper

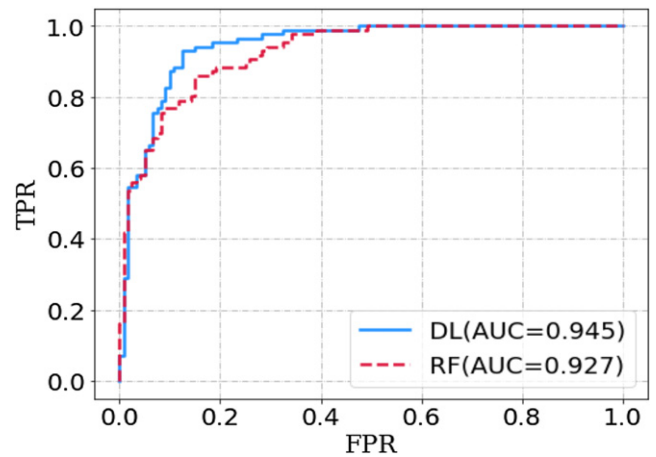


Figure 4. ROC curve of instability predictions for the neural network in a solid blue line and the RF model in a dashed red line on the test set. The area under the ROC curve (AUC)s are 0.945 and 0.927 for the neural network and RF respectively.

left corner (TPR = 1 and FPR = 0) is minimized. At the optimal instability threshold based on the validation dataset, the prediction results on all test data from magnetic EFIT01 equilibria are visualized in figure 5 in physical parameter space. The accuracy (the number of correctly predicted cases divided by the number of all cases) for the neural network and the RF model on the test set is 0.89 and 0.85, respectively. These results demonstrate that SGTC has predictive capabilities for the onset conditions associated with kink modes.

For the second task of SGTC predictions of the mode growth rate, we performed automatic hyperparameter tuning, by randomly generating 100 models in the hyperparameter space. The mean squared error is used as the loss function in this regression problem. After training all 100 models, we select 10 best performing models based on their validation loss, and report the ensemble result of these 10 models. A visualization of the test result is shown in figure 6, where the left panel shows the true value of the growth rate vs the predicted value of the growth rate. The right panel of figure 6 shows a histogram of prediction error. There are some significant under predictions for several test data points with the growth rate greater than 200 kHz. The accuracy of the prediction decreases when the growth rate becomes large, possibly due to the small number of training data in the large growth rate regime, as shown in the histogram of growth rate in figure 2. In figure 7, we compared SGTC performance with a simplified analytic formula of the internal kink instability [51] $\gamma \propto k_z^3 V_A r^2 (q=1)$, where k_z denotes the parallel wave number, and V_A denotes the Alfvén velocity. In the left panel of figure 7, we showed a comparison of the mean squared error of the prediction of the growth rate from random guess, the analytic formula and SGTC for all the data in the test set. The random guess is randomly generated values from uniform distribution ranging from 0–10 kHz, where 10 kHz is around the mean growth rate of the unstable cases. The error bar is the standard deviation divided by the square root of the number of test data points. We normalized the analytic formula such that the mean growth rate on the test set matches the true value, which is not

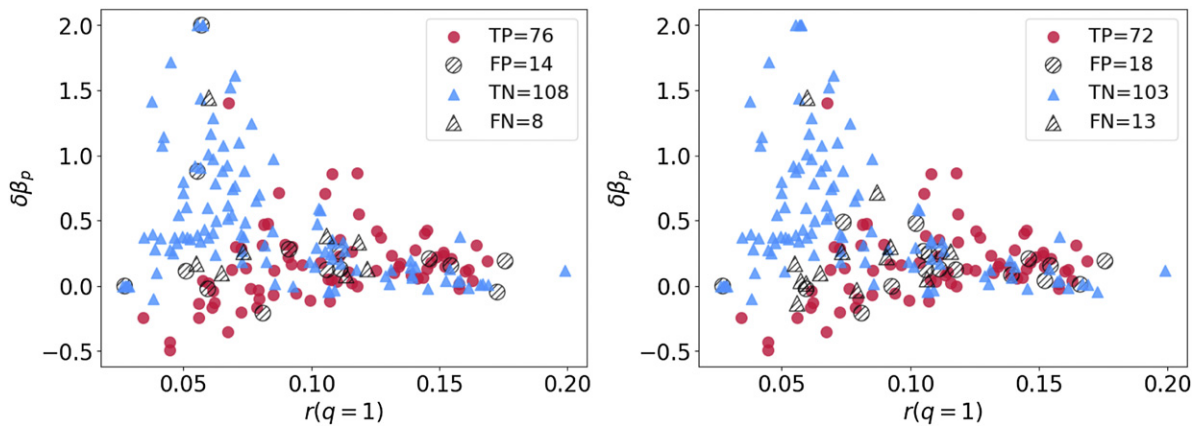


Figure 5. Prediction of kink instability on test dataset from DL method in the left panel and RF method in the right panel. Solid red dot represents the true positive (TP), solid blue triangle represents the true negative (TN), shaded circles represent the false positive (FP), and shaded triangles represent the false negative (FN).

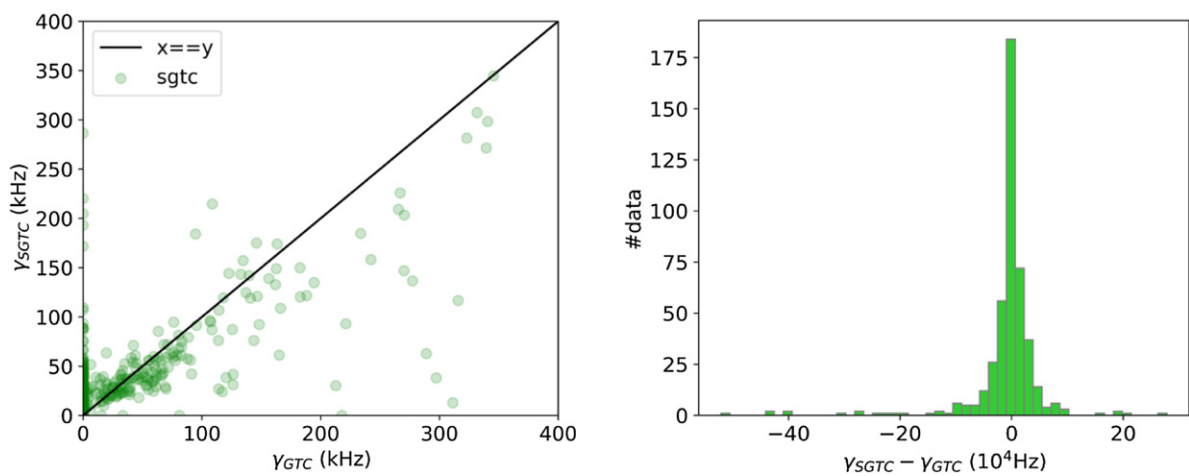


Figure 6. Prediction results of the kink growth rate for entire test dataset. The left panel visualizes the true value of the growth rate vs the predicted value of the growth rate. The solid black line indicates $x = y$ where perfect predictions occur. The right panel shows a histogram of prediction error.

available in realistic scenarios, therefore the analytic formula should be considered ‘boosted’. The high error level of the analytic formula from GTC results shows that GTC simulation of the kink mode in the MHD limit for realistic DIII-D geometry yields significantly different results from simplified analytic estimations. The mean squared error of SGTC predictions of the mode growth rate for the test dataset is $4.4 \times 10^3 \text{ kHz}^2$, significantly lower than the analytic formula estimation. In the right panel of figure 7, we compared the mean squared error of the prediction of the growth rate for unstable cases with growth rate smaller than 50 kHz. The yellow bar represents the difference between GTC simulation and simulation result from four other MHD codes M3D-C1, GAM-solver, NOVA, and XTOR-K [45] for the DIII-D shot number 141216 at 1750 ms, which has unstable kink mode in the MHD limit with a growth rate around 50 kHz. The details of this benchmark is presented in [45]. These results show that SGTC has predictive capabilities for the kink linear growth rate. With more training data and advanced algorithms, its performance can be further improved to better represent GTC simulation results.

We would like to highlight that the average inference time of the ensemble model on NVIDIA V100 GPUs is 0.88 ms. With parallel algorithms, this inference model would fit the run time requirement of the DIII-D PCS. This facilitates the incorporation of the physics-based instability information from the first-principles based global electromagnetic simulations into the PCS of modern tokamaks.

For the third task of the SGTC predictions of the poloidal mode structure, we used the linear mode structure of the perturbed electrostatic potential and perturbed parallel vector potential from GTC simulations as the SGTC model outputs. Examples of the poloidal mode structures from GTC simulations are shown in the upper panels of figure 8. We tuned the hyperparameter automatically by training 10 models in the random hyperparameter space, and selecting the model with the minimum validation loss. Visualization of the SGTC prediction of the mode structure is shown in the lower panels of figure 8. A qualitative agreement is achieved for about 85% of the test dataset. An example where SGTC predictions of the mode structures agree well with the GTC output is

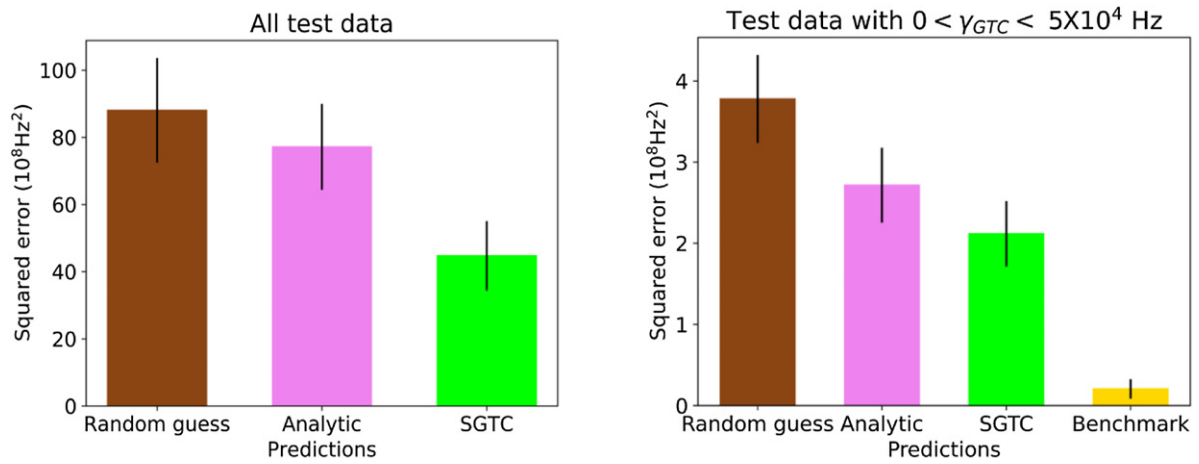


Figure 7. Comparison of SGTC performance for all test dataset with random guess and analytic formula in the left panel. Right panel shows the comparison of SGTC performance with random guess, analytic formula for test data with kink growth rate smaller than 50 kHz. Yellow bar represents the difference between GTC and four other MHD-based simulations [45] for DIII-D shot #141216 at 1750 ms.

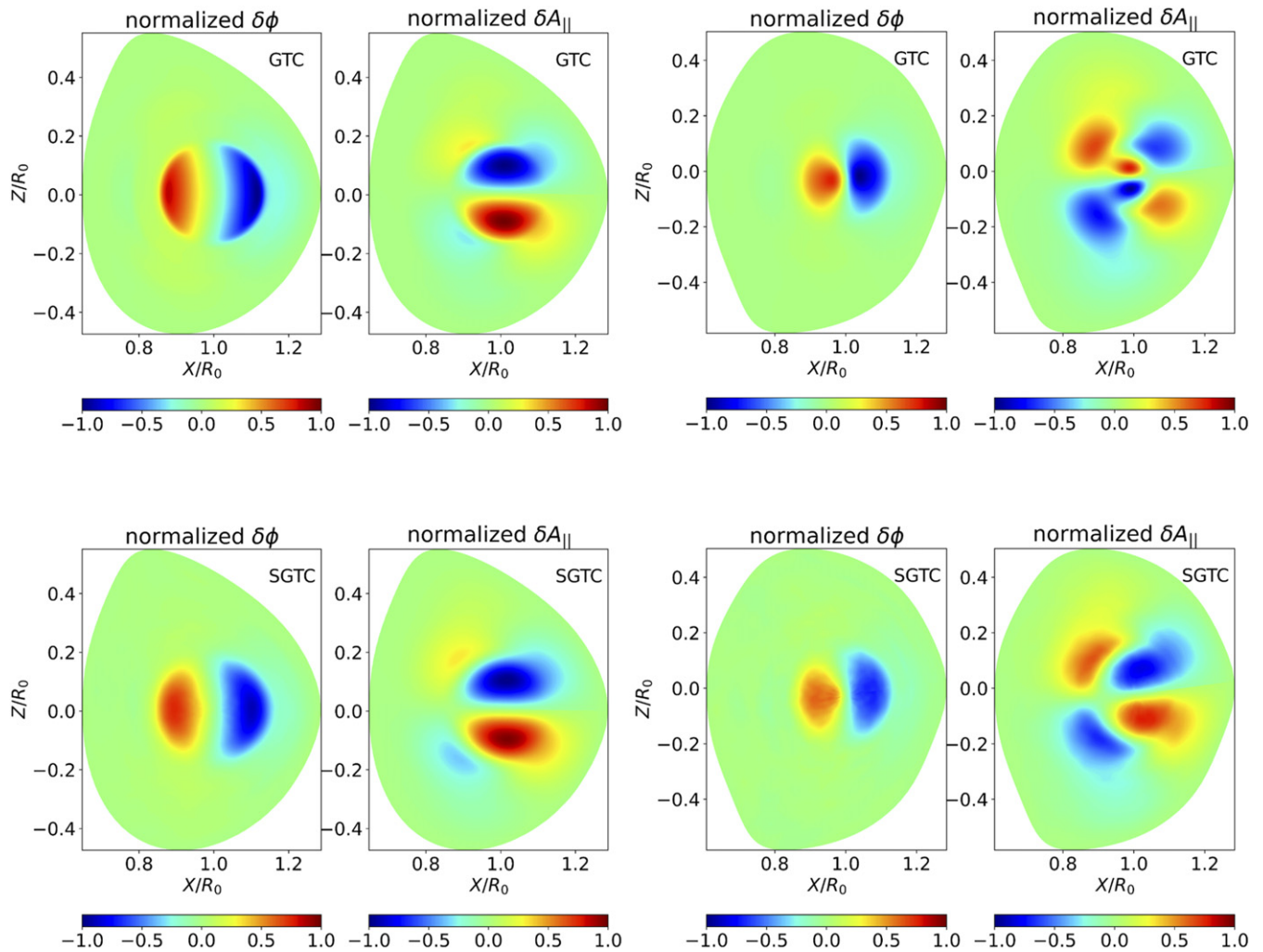


Figure 8. Example of SGTC prediction results of the mode structure of shot #162930 at 1820 ms using magnetic EFIT01 reconstruction in the left 4 panels and shot #140510 at 3145 ms in the right 4 panels using MSE EFIT02 equilibrium reconstruction. Upper panels are GTC outputs and lower panels are SGTC outputs.

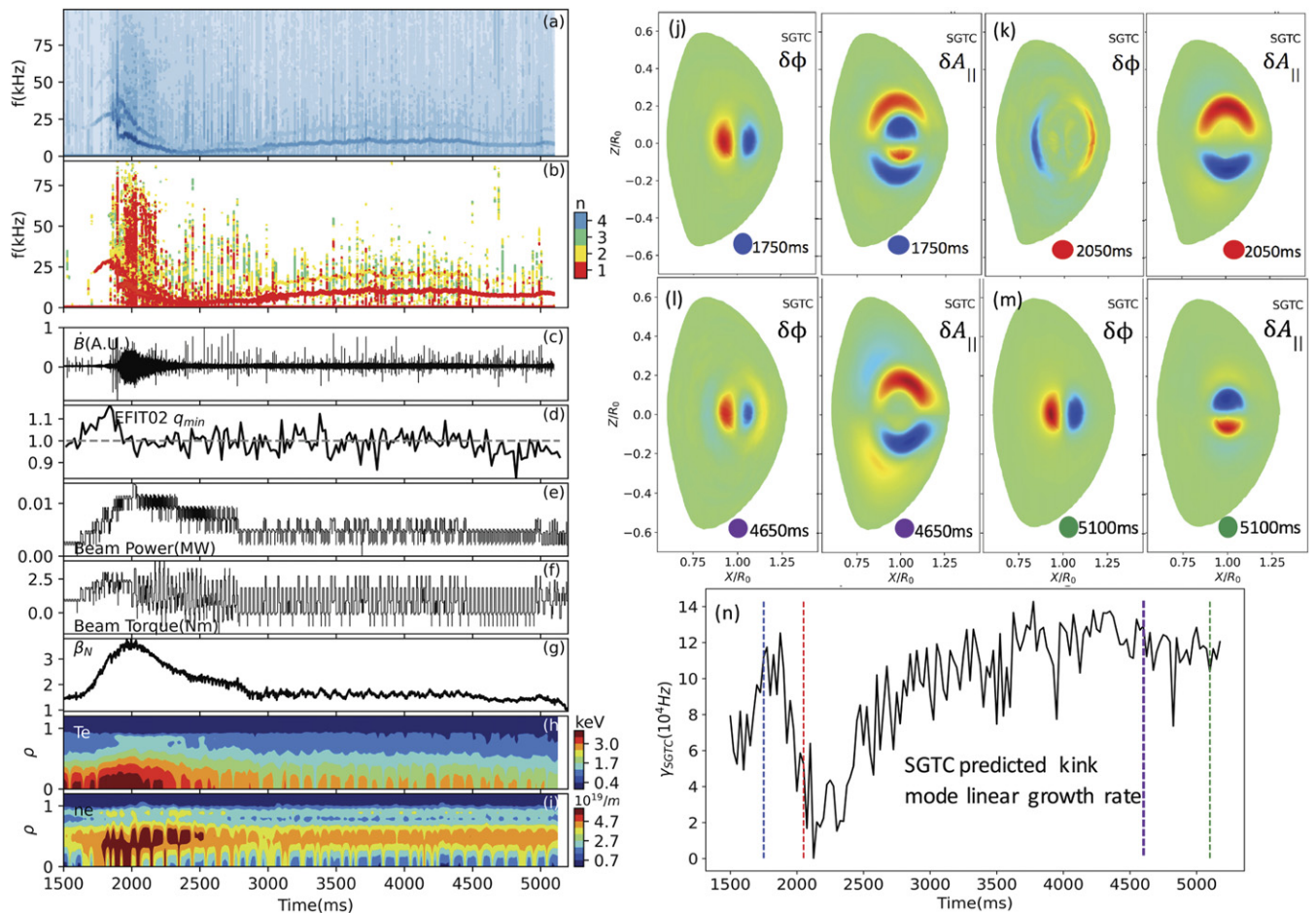


Figure 9. SGTC prediction of internal kink mode linear properties for shot #141216. Left panels show plasma signals from experimental measurements. Magnetic spectrograms from the Mirnov coils are shown in panels (a) and (b), where (b) shows the toroidal mode number n calculated from two coils. Panels (c)–(i) show magnetic perturbation amplitude, minimum safety factor from MSE EFIT02 equilibrium reconstruction, total input beam power, total input beam torque, normalized plasma beta, plasma temperature profile and plasma density profile respectively. The SGTC predicted time evolution of the internal kink mode growth rate is shown in panel (n), and the predicted mode structures for time slices 1750 ms, 2050 ms, 4650 ms and 5100 ms are shown in panels (j)–(m) respectively.

demonstrated in the left panels of figure 8. The right panels of figure 8 show GTC and SGTC output of the poloidal mode structure for the equilibrium in shot #140510 at 3145 ms, where SGTC provides correct predictions for the mode structure in most parts of the simulation domain, but misses the fine structure near the magnetic axis. The SGTC prediction is actually a more ‘typical’ internal kink mode structure compared to the ground truth. That means the model has learned the mode structure features statistically. In both cases, the model learns the importance of $q = 1$ surface to the mode structure. As the low mode number kink linear structure is relatively simple, we still used the standard mean squared error as the loss function, and did not quantitatively define a ‘good’ prediction for the mode structure. Beyond the scope of this paper, for the predictions for instabilities involving more complicated mode structures in future work, we can use unsupervised training algorithms such as clustering to more carefully define a mode structure predictive capability.

Finally, SGTC can be applied to simulate the entire duration of the DIII-D experiments for linear analysis of the internal kink mode onset. The inference for large amount of archived experimental data can provide useful database for statistical analysis. An example of SGTC ‘simulation’ of the internal kink linear mode structure evolution for shot # 141216 from 1500 ms to 5200 ms is shown in figure 9. The left panels show the evolution of measured physical parameters, and the right panels show SGTC outputs. SGTC output shows that the $n = 1$ kink mode is linearly unstable for most part of the shot, except at around 2–2.5 s when the growth rate decreases. The mode structure shifts between $q = 1$ and $q = 2$ surfaces. This result can be qualitatively consistent with observations such as the Mirnov coil data. Since SGTC in this work is limited to the onset conditions and linear properties of the mode, some of the prediction results cannot be compared directly with experimental observations, which are primarily nonlinear in character. Realistic equilibrium and instability scenarios are

complicated by the fishbone modes, tearing modes, the kinetic effects and nonlinear dynamics of all the instabilities, which SGTC will be trained and tested on in future studies.

5. Conclusions and discussions

In this work we designed and constructed a framework for DL based surrogate models for first-principles global electromagnetic toroidal plasma simulations. As a demonstration of this new tool, we simulated 5758 DIII-D equilibria using GTC in the MHD limit. The surrogate models of GTC (SGTC) are trained to predict for the linear properties of the $n = 1$ current driven internal kink instabilities in DIII-D plasmas. The SGTC linear internal kink simulators demonstrate predictive capabilities for the GTC linear simulations that captures the kink mode onset conditions. SGTC shortens the simulation time by at least six orders of magnitude, and presents for the first time the possibility of bringing physics-based instability information from the first-principles based massively parallel simulations into the PCS of modern tokamaks.

This paper focuses on comparing SGTC output with GTC simulations results, as shown in figures 4 to 8. Since the GTC simulation model used in this work is in the ideal MHD limit in the linear kink simulations, without kinetic effects, energetic particle effects, sheared flow, nonlinear dynamics etc, the training data and prediction results may not be realistic in quantitative comparison with experimental data. This work demonstrates the verification of SGTC against GTC results for the onset of the internal kink modes, and the equilibrium database used in this work is based on magnetic EFIT01 and MSE EFIT02. For validation against experimental data in next-step work, kinetic equilibrium reconstructions [49] will be considered. In the future, SGTC can be trained to output the instability properties of the fishbone, tearing mode, Alfvén eigenmode, and microturbulence, together with their nonlinear dynamics and transport levels. The methodology of SGTC can also be applied to training emulators for other first-principle plasma simulations such as the MHD codes.

Finally, we would like to highlight that although the capabilities of current simulation tools are still limited in many challenging aspects such as the nonlinear modeling of the full experimental plasma scenarios, current first-principles simulations are extremely useful in uncovering the physics in fusion plasmas and are absolutely necessary for the prediction of plasma conditions in future tokamaks such as ITER. Therefore, the advancements of these simulations using modern computational and statistical methods, such as the SGTC framework (which provided a path to the fundamental advancement in simulation time to allow real-time applications) that this paper is initiating, can be valuable for the fusion community.

Acknowledgments

We would like to thank Dr. William Heidbrink, Dr. Brian Victor, Dr. Jayson Barr and other colleagues for their support and helpful discussions. GTC runs in this work

are performed on Summit. Neural networks in SGTC framework are trained on Summit (<https://olcf.ornl.gov/olcf-resources/compute-systems/summit/>), tigergpu (<https://researchcomputing.princeton.edu/systems/tiger>) and traverse (<https://researchcomputing.princeton.edu/systems/traverse>).

This work is supported by the U.S. Department of Energy (DOE) SciDAC project ISEP and used resources of the Oak Ridge Leadership Computing Facility at Oak Ridge National Laboratory (DOE Contract No. DE-AC05-00OR22725) and the National Energy Research Scientific Computing Center (DOE Contract No. DE-AC02-05CH11231).

This work is partially based upon work using the DIII-D National Fusion Facility, a DOE Office of Science user facility, under Awards DE-FC02-04ER54698. This report was prepared as an account of work sponsored by an agency of the United States Government. Neither the United States Government nor any agency thereof, nor any of their employees, makes any warranty, express or implied, or assumes any legal liability or responsibility for the accuracy, completeness, or usefulness of any information, apparatus, product, or process disclosed, or represents that its use would not infringe privately owned rights. Reference herein to any specific commercial product, process, or service by trade name, trademark, manufacturer, or otherwise, does not necessarily constitute or imply its endorsement, recommendation, or favoring by the United States Government or any agency thereof. The views and opinions of authors expressed herein do not necessarily state or reflect those of the United States Government or any agency thereof.

ORCID iDs

G. Dong  <https://orcid.org/0000-0002-7734-3736>

X. Wei  <https://orcid.org/0000-0001-7486-0407>

References

- [1] Strait E.J. et al 2019 Progress in disruption prevention for ITER *Nucl. Fusion* **59** 112012
- [2] La Haye R.J. 2006 Neoclassical tearing modes and their control *Phys. Plasmas* **13** 055501
- [3] de Vries P.C., Johnson M.F., Alper B., Buratti P., Hender T.C., Koslowski H.R. and Riccardo V. (JET-EFDA Contributors) 2011 Survey of disruption causes at JET *Nucl. Fusion* **51** 053018
- [4] Sauter O. et al 2002 Control of neoclassical tearing modes by sawtooth control *Phys. Rev. Lett.* **88** 105001
- [5] Chapman I.T. et al 2012 Sawtooth control using electron cyclotron current drive in ITER demonstration plasmas in DIII-D *Nucl. Fusion* **52** 063006
- [6] ITER Organization ITER—the way to new energy 2021 available at <https://iter.org/>
- [7] Hawryluk R.J. and Zohm H. 2019 The challenge and promise of studying burning plasmas *Phys. Today* **72** 34
- [8] Lin Z., Ethier S., Hahn T.S. and Tang W.M. 2002 Size scaling of turbulent transport in magnetically confined plasmas *Phys. Rev. Lett.* **88** 195004
- [9] Jardin S.C., Ferraro N. and Krebs I. 2015 Self-organized stationary states of tokamaks *Phys. Rev. Lett.* **115** 215001

- [10] Groebner R.J. *et al* 2013 Improved understanding of physics processes in pedestal structure, leading to improved predictive capability for ITER *Nucl. Fusion* **53** 093024
- [11] Chang C.S. *et al* 2017 Gyrokinetic projection of the divertor heat-flux width from present tokamaks to ITER *Nucl. Fusion* **57** 116023
- [12] Cheng C.Z. 1992 Kinetic extensions of magnetohydrodynamics for axisymmetric toroidal plasmas *Phys. Rep.* **211** 1–51
- [13] Breslau J., Ferraro N. and Jardin S. 2009 Some properties of the M3D-C1 form of the three-dimensional magnetohydrodynamics equations *Phys. Plasmas* **16** 092503
- [14] Kotschenreuther M., Rewoldt G. and Tang W.M. 1995 Comparison of initial value and eigenvalue codes for kinetic toroidal plasma instabilities *Comput. Phys. Commun.* **88** 128–40
- [15] Holland C., Petty C.C., Schmitz L., Burrell K.H., McKee G.R., Rhodes T.L. and Candy J. 2012 Progress in GYRO validation studies of DIII-D H-mode plasmas *Nucl. Fusion* **52** 114007
- [16] Lin Z., Hahm T.S., Lee W.W., Tang W.M. and White R.B. 1998 Turbulent transport reduction by zonal flows: massively parallel simulations *Science* **281** 1835
- [17] Chang C.S., Ku S. and Weitzner H. 2004 Numerical study of neoclassical plasma pedestal in a tokamak geometry *Phys. Plasmas* **11** 2649
- [18] Taimourzadeh S. *et al* 2019 Verification and validation of integrated simulation of energetic particles in fusion plasmas *Nucl. Fusion* **59** 066006
- [19] Wang W.X., Lin Z., Tang W.M., Lee W.W., Ethier S., Lewandowski J.L.V., Rewoldt G., Hahm T.S. and Manickam J. 2005 Global gyrokinetic particle simulation of turbulence and transport in realistic tokamak geometry *J. Phys.: Conf. Ser.* **16** 008
- [20] Madduri K. *et al* 2011 Gyrokinetic toroidal simulations on leading multi- and manycore HPC systems *SC '11: Proc. 2011 Int. Conf. High Performance Computing, Networking, Storage and Analysis* (Seattle, Washington, USA, 12–18 November 2011) pp 1–12
- [21] Rea C., Montes K. J., Erickson K. G., Granetz R. S. and Tinguely R. A. 2019 A real-time machine learning-based disruption predictor in DIII-D *Nucl. Fusion* **59** 096016
- [22] Fu Y. *et al* 2020 Machine learning control for disruption and tearing mode avoidance *Phys. Plasmas* **27** 022501
- [23] Kates-Harbeck J., Svyatkovskiy A. and Tang W. 2019 Predicting disruptive instabilities in controlled fusion plasmas through deep learning *Nature* **568** 526–31
- [24] Lyons B.C., Paz-Soldan C., Meneghini O., Lao L.L., Weisberg D.B., Belli E.A., Evans T.E., Ferraro N.M. and Snyder P.B. 2018 Predict-first experimental analysis using automated and integrated magnetohydrodynamic modeling *Phys. Plasmas* **25** 056111
- [25] Miller M.A., Churchill R.M., Dener A., Chang C.S., Munson T. and Hager R. 2020 Encoder–decoder neural network for solving the nonlinear Fokker–Planck–Landau collision operator in XGC (arXiv:2009.06534)
- [26] Wong K.L. *et al* 2000 Internal kink instability during off-axis electron cyclotron current drive in the DIII-D tokamak *Phys. Rev. Lett.* **85** 996
- [27] Menard J.E. *et al* 2005 Internal kink mode dynamics in high- β NSTX plasmas *Nucl. Fusion* **45** 539
- [28] Xu L. *et al* 2012 Observations of pressure gradient driven $m = 1$ internal kink mode in EAST tokamak *Phys. Plasmas* **19** 122504
- [29] Porcelli F., Boucher D. and Rosenbluth M.N. 1996 Model for the sawtooth period and amplitude *Plasma Phys. Control. Fusion* **38** 2163
- [30] Heidbrink W.W. and Sager G. 1990 The fishbone instability in the DIII-D tokamak *Nucl. Fusion* **30** 1015
- [31] Wang F., Fu G.Y., Breslau J.A., Tritz K. and Liu J.Y. 2013 Simulation of non-resonant internal kink mode with toroidal rotation in the national spherical torus experiment *Phys. Plasmas* **20** 072506
- [32] Chang Z., Callen J.D., Fredrickson E.D., Budny R.V., Hegna C.C., McGuire K.M. and Zarnstorff M.C. (TFTR Group) 1995 Observation of nonlinear neoclassical pressure-gradient-driven tearing modes in TFTR *Phys. Rev. Lett.* **74** 4663
- [33] Sainath T.N., Vinyals O., Senior A. and Sak H. 2015 Convolutional, long short-term memory, fully connected deep neural networks 2015 *IEEE Int. Conf. Acoustics, Speech and Signal Processing (ICASSP)* (South Brisbane, QLD, Australia, 19–24 April 2015) pp 4580–4
- [34] Lin Z., Tang W.M. and Lee W.W. 1995 Gyrokinetic particle simulation of neoclassical transport *Phys. Plasmas* **2** 2975
- [35] Lee W.W., Tang W.M., Diamond P.H., Lin Z. and Hahm T.S. 1999 Effects of collisional zonal flow damping on turbulent transport *Phys. Rev. Lett.* **83** 3645
- [36] Lin Z., Tang W.M. and Lee W.W. 1997 Neoclassical transport in enhanced confinement toroidal plasmas *Phys. Rev. Lett.* **78** 456
- [37] Lin Z., Holod I., Chen L., Diamond P.H., Hahm T.S. and Ethier S. 2007 Wave-particle decorrelation and transport of anisotropic turbulence in collisionless plasmas *Phys. Rev. Lett.* **99** 265003
- [38] Zhang W., Lin Z. and Chen L. 2008 Transport of energetic particles by microturbulence in magnetized plasmas *Phys. Rev. Lett.* **101** 095001
- [39] Xiao Y. and Lin Z. 2009 Turbulent transport of trapped electron modes in collisionless plasmas *Phys. Rev. Lett.* **103** 085004
- [40] Zhang H.S., Lin Z. and Holod I. 2012 Nonlinear frequency oscillation of Alfvén eigenmodes in fusion plasmas *Phys. Rev. Lett.* **109** 025001
- [41] Wang Z., Lin Z., Holod I., Heidbrink W.W., Tobias B., Van Zeeland M. and Austin M.E. 2013 Radial localization of toroidicity-induced Alfvén eigenmodes *Phys. Rev. Lett.* **111** 145003
- [42] Schmitz L. *et al* 2016 Suppressed ion-scale turbulence in a hot high- β plasma *Nat. Commun.* **7** 13860
- [43] Xie H.S., Xiao Y. and Lin Z. 2017 New paradigm for turbulent transport across a steep gradient in toroidal plasmas *Phys. Rev. Lett.* **118** 095001
- [44] McClenaghan J., Lin Z., Holod I., Deng W. and Wang Z. 2014 Verification of gyrokinetic particle simulation of current-driven instability in fusion plasmas: I. Internal kink mode *Phys. Plasmas* **21** 122519
- [45] Brochard G. *et al* 2021 Verification and validation of gyrokinetic and kinetic-MHD simulations for internal kink instability in DIII-D tokamak (arXiv:2109.09891)
- [46] Holod I., Zhang W. L., Xiao Y. and Lin Z. 2009 Electromagnetic formulation of global gyrokinetic particle simulation in toroidal geometry *Phys. Plasmas* **16** 122307
- [47] Dong G., Bao J., Bhattacharjee A., Brizard A., Lin Z. and Porazik P. 2017 Gyrokinetic particle simulations of the effects of compressional magnetic perturbations on drift-Alfvénic instabilities in tokamaks. *Phys. Plasmas* **24** 081205
- [48] Lao L.L., John H. St, Stambaugh R.D., Kellman A.G. and Pfeiffer W. 1985 Reconstruction of current profile parameters and plasma shapes in tokamaks *Nucl. Fusion* **25** 1611
- [49] Lao L.L., John H.E.S., Peng Q., Ferron J.R., Strait E.J., Taylor T.S., Meyer W.H., Zhang C. and You K.I. 2005 MHD

- equilibrium reconstruction in the DIII-D tokamak *Fusion Sci. Technol.* **48** 968–77
- [50] Wei X. *et al* 2021 Electromagnetic formulations for GTC simulation (arXiv:2109.08873)
- [51] Rosenbluth M.N., Dagazian R.Y. and Rutherford P.H. 1973 Nonlinear properties of the internal $m = 1$ kink instability in the cylindrical tokamak *Phys. Fluids* **16** 1894
- [52] Wróblewski D. and Lao L.L. 1992 Polarimetry of motional Stark effect and determination of current profiles in DIII-D (invited) *Rev. Sci. Instrum.* **63** 5140
- [53] White R.B. and Chance M.S. 1984 Hamiltonian guiding center drift orbit calculation for plasmas of arbitrary cross section *Phys. Fluids* **27** 2455
- [54] Bussac M.N., Pellat R., Edery D. and Soule J.L. 1975 Internal kink modes in toroidal plasmas with circular cross sections *Phys. Rev. Lett.* **35** 1638
- [55] scikit-learn developers 2021 *sklearn.ensemble.RandomForestRegressor* (<https://scikit-learn.org/stable/modules/generated/sklearn.ensemble.RandomForestRegressor.html>) (15 September 2021)